Chemical Engineering Journal 95 (2003) 1–13

Chemical Engineering Journal

www.elsevier.com/locate/cej

Hydrodynamic simulation of gas–solid flow in a riser using kinetic theory of granular flow

Lu Huilin [a,*], Dimitri Gidaspow [b], Jacques Bouillard [c], Liu Wentie [a]

[a] *Department of Power Engineering, Harbin Institute of Technology, Harbin 150001, PR China*
[b] *Department of Chemical and Environmental Engineering, Illinois Institute of Technology, Chicago, IL 60616, USA*
[c] *INERIS, Parc ALATA, BP 2, Verneuil en Halatte 60550, France*

Received 5 July 2002; accepted 27 January 2003

Abstract

The dynamic behavior of gas–solids flow in a 6-m high riser was predicted using a transient two-dimensional (2D) hydrodynamic model based on the kinetic theory of granular flows. Instantaneous and local gas-particle velocity, void fraction and turbulent parameters were obtained. Predicted time-averaged particle concentrations and velocities reflect the classical core-annular flow structure in agreement with experimental measurements, in particular, with those reported by Miller and Gidaspow [AIChE J. 38 (1992) 1801]. Predicted instantaneous solids concentration frequencies compared well with the experimental data for various regions of the riser. Computed total granular temperature distributions in the riser qualitatively agree with experimental data. High thermal conductivities of fluidized powders (about 50 times that of the fluidizing gas) were estimated from the kinetic theory without adjusted parameters. Effects of initial conditions, inlet geometry, riser diameter and riser vertical inclination were assessed. Unexpected strong distortions of solids concentrations and vertical fluxes were predicted for small inclination angles of the order of 2°. Analysis of experimental data should, therefore, be carefully conducted to ensure that riser inclination is not too important over the length of the riser in order to eliminate potential artifacts due to this geometric parameter.

Keywords: Gas–solids two-phase flow; Kinetic theory of granular flow; Numerical simulation; Hydrodynamics

1. Introduction

Circulating fluid beds have been widely applied in various industrial practices including fluid catalytic cracking, calcination of alumina trihydrate to high-purity alumina, combustion of low-grade coal in power generation. A quantitative understanding of the performance of these processes hinges on our ability to capture the complex hydrodynamics observed in them. Several modeling effects employing very different mathematical formulations have appeared in the recent literature to predict the relationship between solids concentration, operating conditions, and riser geometry. The first step in the fundamental understanding of fluidization is usually attributed to Davidson [1] for his analysis of a single bubble motion in an infinite fluid bed. Arastoopour and Gidaspow [2] established four different two-phase flow models for the description of one-dimensional steady-state pneumatic conveying systems. The model with solids viscosity as an input was first used by Tsuo and Gidaspow [3] in the simulations of gas–solids flow in riser. They predicted the cluster formation and the core-annular flow using a two-dimensional (2D) gas–solids flow model. Lyczkowsky et al. [4] and Anderson et al. [5] simulated the flow of gas–solids mixture in the bubbling fluidized bed using the viscosity value based on experimental measurements to model the viscous effects of the solids phase. Benyahia et al. [6] and Sun and Gidaspow [7] predicted the gas–solids flow in the circulating fluidized beds using the viscosity data from Miller and Gidaspow's experiments [8].

In recent years, one step forward in the understanding of gas–solids systems has been taken by the development of kinetic theory for gas–solids two-phase flow based on the theory for non-uniform dense gases described in Chapman and Cowling [9]. The pioneering paper of Lun et al. [10] applied the kinetic theory of gases to granular flow. The kinetic theory approach uses a one equation model to determine the turbulent kinetic energy (or granular temperature) of the particles and assumes either a Maxwellian distribution for the particles, or a non-Maxwellian distribution for both dilute and dense cases. The kinetic theory approach for granular flow allows the determination of the pressure and

* Corresponding author.
E-mail address: huilin@hope.hit.edu.cn (L. Huilin).

1385-8947/$ – see front matter © 2003 Elsevier Science B.V. All rights reserved.
doi:10.1016/S1385-8947(03)00062-7

Nomenclature

C_d	drag coefficient
d	particle diameter
D	diameter of riser
D_{gs}	rate of energy dissipation
e	restitution coefficient of particles (= 0.999)
e_w	restitution coefficient of wall (= 0.96)
G_s	solid mass flux
$\boldsymbol{g}$	gravity
g_0	radial distribution function
G_s	solid flux
$\boldsymbol{I}$	unit tensor
k_s	effective thermal conductivity of particles
k_g	thermal conductivity of gas phase
n	normal direction
N	sampling number
$\boldsymbol{P}_g$	pressure
$\boldsymbol{P}_s$	particle pressure
q	fluctuating energy flux
Re	Reynolds number
r	radial coordinate
t	time
$\boldsymbol{v}_g$	gas velocity
$\boldsymbol{v}_s$	particle velocity
u_g	gas velocity
z	axial coordinate

Greek letters

τ_g	gas stress tensor
τ_s	stress tensor of particulate phase
ξ	bulk viscosity
θ	granular temperature
μ_g	gas viscosity
μ_s	particulate viscosity
ε_g	voidage
ε_s	solid volume fraction
ρ_s	particle density
ρ_g	gas density
β	interphase drag coefficient

viscosity of the solids in place of empirical relations. Sinclair and Jackson [11] applied the granular flow model to a fully developed gas–solids flow in a pipe. Ding and Gidaspow [12] derived expressions for solids viscosity and pressure of a dense gas–solids flow. Gidaspow extend the Ding and Gidaspow [12] formulation to both dilute and dense cases by considering a non-Maxwellian velocity distribution [13]. Louge et al. [14], Pita and Sundareasan [15] and Hrenya and Sinclair [16] incorporated the effects of gas turbulence into their models by modifying single-phase turbulence closures to account for the presence of particle phase. Samuelsberg and Hjertager [17] included both gas turbulence by using LES method and particle–particle interaction using the kinetic theory approach. Nieuwland et al. [18], Balzer et al. [19] and Neri and Gidaspow [20] conducted simulations of gas–solids flow in the circulating fluidized bed using kinetic theory of granular flow.

In the present study, the kinetic theory approach considering the effect of the interaction of particle and gas phase, and particle collisions has been applied to the study of a gas–solids flow in the riser of circulating fluidized beds. The flow pattern has been investigated by a transient 2D two-fluid model. The model was used to reproduce two-phase flow experiments performed by Miller and Gidaspow [8]. Such experiments have already been the subject of several investigations [20,21] and, in some cases, a good agreement between prediction and experimental data was obtained. This experimental data set is used in this study because it is believed to be a relatively complete hydrodynamic set on pressure distribution, solids concentration, velocity, mass flux, granular temperature and pressure and for which key parameters such as the particle–particle restitution and particle–wall restitution coefficients have been measured. The purpose of this study is to extend the comparisons between model predictions and experimental data previously done by other investigators in light of these new parameter estimates. In addition, emphasis is particularly placed on the effect of the riser inlet configuration, initial condition, diameter of riser, riser inclination angle, as well as on the analysis of the oscillations characterizing the riser dynamics.

Simulation results are able to describe the main features of the gas–solids flow patterns in the riser, such as the core-annular flow regime. Frequency analysis of the oscillatory gas–solids flow were performed to analyze the riser dynamics. Agreement between predictions and experimental data are reasonably good which allows us to become more confident with the adopted theory and computer code. The governing equations, numerical method, and simulation results are presented in the following sections.

2. Gas–solids flow model description

The model adopted is based on the fundamental concept of interpenetrating continua for multiphase mixtures. According to this theory different phases can be present at the same time in the same computational volume. Such an idea is made possible by the introduction of a new dependent variable, the concentration, ε_i, of each phase i. The fundamental equations of mass, momentum, and energy conservation are then solved for each considered phase. Appropriate constitutive equations have to be specified in order to describe the physical rheological properties of each phase and to close the conservation equations. In this model, solids viscosity and pressure are derived by considering the random fluctuation of particle velocity and its variations due to particle–particle collisions and the actual flow field. Such a random kinetic energy, or granular temperature, can be predicted by solving, in addition to the mass and

momentum equations, a fluctuating kinetic energy equation for the particles. The solids viscosity and pressure can then be computed as a function of granular temperature at any time and position. Particles are considered smooth, spherical, inelastic, and undergoing binary collisions. The adoption of the second approximation distribution function allows us to apply the theory to both dense and dilute two-phase flows. A more complete discussion of the implemented kinetic theory model can be found in Gidaspow [13].

2.1. Continuity and momentum equation

The accumulation of mass in each phase is balanced by the convective mass flows (i = gas, solids):

$$\frac{\partial}{\partial t}(\varepsilon_i \rho_i) + \nabla \cdot (\varepsilon_i \rho_i \boldsymbol{v}_i) = 0 \tag{1}$$

where ε is the concentration of each phases, $\boldsymbol{v}$ the velocity vector, and ρ the density. Mass exchanges between the phases, e.g. due to reaction or combustion, are not considered.

The momentum balance for the gas phase is given by the Navier–Stokes equation, modified to include an interphase momentum transfer term [13]:

$$\frac{\partial}{\partial t}(\varepsilon_g \rho_g \boldsymbol{v}_g) + \nabla \cdot (\varepsilon_g \rho_g \boldsymbol{v}_g \boldsymbol{v}_g) = \nabla \cdot \boldsymbol{\tau}_g + \varepsilon_g \rho_g \boldsymbol{g} - \nabla p - \beta(\boldsymbol{v}_g - \boldsymbol{v}_s) \tag{2}$$

where $\boldsymbol{g}$ is the gravity acceleration, p the thermodynamic pressure, β the interface momentum transfer coefficient, and $\boldsymbol{\tau}_g$ the viscous stress tensor. The stress tensor of gas phase can be represented as:

$$\boldsymbol{\tau}_g = \mu_g[\nabla \boldsymbol{v}_g + (\nabla \boldsymbol{v}_g)^T] - \tfrac{2}{3}\mu_g(\nabla \cdot \boldsymbol{v}_g)\boldsymbol{I} \tag{3}$$

The gas phase turbulence is modeled by the Sub Grid Scale (SGS) model, and thus the gas shear viscosity may be estimated as [22]:

$$\mu_g = \mu_{g,l} + \rho_g (0.1\Delta)^2 (\boldsymbol{\tau}_g \cdot \boldsymbol{\tau}_g) \tag{4}$$

$$\Delta = (\Delta x \Delta y \Delta z)^{1/2} \tag{5}$$

The solids phase momentum balance is given by [13]:

$$\frac{\partial}{\partial t}(\varepsilon_s \rho_s \boldsymbol{v}_s) + \nabla \cdot (\varepsilon_s \rho_s \boldsymbol{v}_s \boldsymbol{v}_s) = \nabla \cdot \bar{\boldsymbol{\tau}}_s + \varepsilon_s \rho_s \boldsymbol{g} + \beta(\boldsymbol{v}_g - \boldsymbol{v}_s) \tag{6}$$

The solids stress tensor can be expressed in terms of the solids pressure, P_s; bulk solids viscosity, ξ_s; and shear solids viscosity, μ_s; as

$$\tau_s = (-\boldsymbol{P}_s + \xi_s \nabla \cdot \boldsymbol{v}_s)\boldsymbol{I} + \mu_s\{[\nabla \boldsymbol{v}_s + (\nabla \boldsymbol{v}_s)^T] - \tfrac{2}{3}(\nabla \cdot \boldsymbol{v}_s)\boldsymbol{I}\} \tag{7}$$

2.2. Kinetic theory of granular flow

There are two possible mechanisms inducing the fluctuations of particle velocity: inter-particle collisions and particle interactions with turbulent fluctuations in the gas phase. Inter-particle collisions play a crucial role in sufficiently dense suspensions. Equivalent to the thermodynamic temperature for gases, the granular temperature can be introduced as a measure for the energy of the fluctuating velocity of the particles [13]. The granular temperature, θ, is defined as: $\theta = \boldsymbol{v}'^2/3$, where $\boldsymbol{v}'$ is the particle fluctuating velocity. The equation of conservation of solids fluctuating energy can be found [13]:

$$\frac{3}{2}\left[\frac{\partial}{\partial t}(\varepsilon_s \rho_s \theta) + \nabla \cdot (\varepsilon_s \rho_s \theta)\boldsymbol{v}_s\right] = (-\nabla p_s \bar{I} + \tau_s) : \nabla \boldsymbol{v}_s + \nabla \cdot (k_s \nabla \theta) - \gamma_s + \phi_s + D_{gs} \tag{8}$$

where k_s is the thermal conductivity coefficient of solids phase, γ_s the dissipation of fluctuating energy, ϕ_s the exchange of fluctuating energy between the phases, and $\boldsymbol{I}$ the unit tensor. The last two terms in Eq. (8) represent the interaction between gas turbulence and particle fluctuation.

The dissipation fluctuating energy is [13]:

$$\gamma_s = 3(1 - e^2)\varepsilon_s^2 \rho_s g_o \theta \left(\frac{4}{d}\sqrt{\frac{\theta}{\pi}} - \nabla \cdot \boldsymbol{v}_s\right) \tag{9}$$

where e is the restitution coefficient of particles, d the particle diameter, and g_o the radial distribution function at contact. The radial distribution function, g_o, can be seen as a measure for the probability of inter-particle contact. The equation of Bagnold [23] is used in this work:

$$g_o = \left[1 - \left(\frac{\varepsilon_s}{\varepsilon_{s,max}}\right)^{1/3}\right]^{-1} \tag{10}$$

where $\varepsilon_{s,max}$ is the maximum particle packing.

The particle pressure represents the particle normal forces due to particle–particle interaction. Its description based on the kinetic theory of granular flow was developed. In this approach, both the kinetic and the collisional influence are taken into account. The kinetic portion describes the influence of particle translations, whereas the collisional term accounts for the momentum transfer by direct collisions [13]. The particle pressure is calculated as follows:

$$p_s = \varepsilon_s \rho_s \theta[1 + 2g_o \varepsilon_s (1 + e)] \tag{11}$$

The shear viscosity accounts for the tangential forces. It was shown by Lun et al. [10] and Gidaspow [13] that it is possible to combine different inter-particle forces and to use a momentum balance similar to that of a true continuous fluid.

In this work, the equation of particle viscosity [13] is

$$\mu_s = \frac{4}{5}\varepsilon_s^2\rho_s d g_o(1+e)\sqrt{\frac{\theta}{\pi}} + \frac{10\rho_s d\sqrt{\pi\theta}}{96(1+e)\varepsilon_s g_o}\left[1+\frac{4}{5}g_o\varepsilon_s(1+e)\right]^2 \quad (12)$$

and the bulk solids viscosity is as follows:

$$\xi_s = \frac{4}{3}\varepsilon_s^2\rho_s d g_o(1+e)\sqrt{\frac{\theta}{\pi}} \quad (13)$$

The term D_{gs} is the rate of energy dissipation per unit volume resulting from the transfer of gas phase fluctuations to the particle phase fluctuations. In this study, the value of D_{gs} was predicted using Koch's expression [24] as follows:

$$D_{gs} = \frac{d\rho_s}{4\sqrt{\pi\theta}}\left(\frac{18\mu_g}{d^2\rho_s}\right)^2 |\boldsymbol{v}_g - \boldsymbol{v}_s|^2 \quad (14)$$

The exchange of fluctuating energy between gas and particles [13] is

$$\phi_s = -3\beta\theta \quad (15)$$

It accounts for loss of granular energy due to friction with the gas.

2.3. Interphase momentum exchange

In order to couple the two momentum balances, a model for the interface force is required. For porosities <0.8, the pressure drop due to friction between gas and particles can be described by the Ergun equation. Thus, the interface momentum transfer coefficient, β, in this porosity range [13] becomes:

$$\beta = 150\frac{\varepsilon_s^2\mu_g}{\varepsilon_g^2 d^2} + 1.75\frac{\rho_g\varepsilon_s}{\varepsilon_g d}|\boldsymbol{v}_g - \boldsymbol{v}_s| \quad (16)$$

for porosity >0.8, such a relation for pressure drop leads to the following expression for the interface momentum transfer coefficient:

$$\beta = \frac{3C_d\varepsilon_g\varepsilon_s\rho_g|\boldsymbol{v}_g - \boldsymbol{v}_s|}{4d}\varepsilon_g^{-2.65} \quad (17)$$

with

$$C_d = \frac{24}{Re}(1+0.15Re^{0.687}) \quad Re < 1000$$

$$C_d = 0.44 \quad Re \geq 1000$$

where Re is the Reynolds number, $Re = d\rho_g\frac{|\boldsymbol{v}_g - \boldsymbol{v}_s|}{\mu_g}$.

2.4. Boundary conditions

At the inlet, all velocities and concentrations of both phases were specified. The pressure was not specified at the inlet because of the incompressible gas phase assumption (relatively low pressure drop system). At the outlet, the pressure was specified (atmospheric). Initially, the velocity of both the gas and particles was set at zero in the riser.

At the wall, the gas tangential and normal velocities were set to zero (no slip condition). The normal velocity of the particles was also set at zero. The following boundary equations apply for the tangential velocity and granular temperature of particles at the wall [11]:

$$v_{t,w} = -\frac{6\mu_s\varepsilon_{s,max}}{\pi\rho_s\varepsilon_s g_o\sqrt{3\theta}}\frac{\partial v_{s,w}}{\partial n} \quad (18)$$

$$\theta_w = -\frac{k_s\theta}{e_w}\frac{\partial\theta_w}{\partial n} + \frac{\sqrt{3}\pi\rho_s\varepsilon_s\boldsymbol{v}_s g_o\theta^{3/2}}{6\varepsilon_{s,max}e_w} \quad (19)$$

where e_w is the restitution coefficient at the wall.

2.5. Simulation code and computation procedures

The simulations were carried out with the CFD code K-FIX which previously used to model the flow in a bubbling fluidized bed [13], and incorporated with kinetic theory of granular flow in this work. This mathematical process is described by Patankar [25]. This software allows free implementation of extra equations, boundary conditions, and differencing schemes. The granular kinetic theory and the granular equations described in the previous section were implemented into this code in this work. For solving the difference equations obtained from the differential equations, the higher order Total Variation Diminishing method (TVD) scheme is used. This TVD scheme incorporates a modification to the higher order upwind scheme for hyperbolic systems. The solution of the pressure from the momentum equations requires a pressure correction equation, correcting the pressure and the velocities after each iteration of the discretised momentum equations. The calculated pressure is used to compute the density of the gas phase.

Several experiments were performed by Miller and Gidaspow [8] at different points and sections of the riser. The riser is cylindrical with the gas and solids phases leaving through a side port located below the top of the riser. The particle feed rate is controlled by a slide valve. The riser is 75 mm in diameter and 6.58 m long. The average particle diameter and density are 75 μm and 1654 kg/m^3, respectively. By measuring granular temperature and particle velocity distributions by means of a CCD camera, Gidaspow and Huilin [26] estimated a value of restitution coefficient of FCC particles in a riser. They found the value of restitution coefficient of particle-wall, e_w, was 0.96. These parameters are the essential inputs to the proposed kinetic theory model. Fig. 1 shows the riser section used in the present numerical simulation of gas–solids flow. Uniform bottom-inlet conditions for the 2D cylindrical riser are assumed. The 2D riser simulations are proposed in order to evaluate the predictive capabilities of the present model. Note that the numerical mesh discretisation spans from $-D/2$ to $D/2$ rather than 0 to $D/2$ as it is usually done for cylindrical coordinates. This technique helps us simulate asymmetrical inlet and outlet boundary conditions keeping the computational workload to a reasonable level. Such 2D simulations can be used for

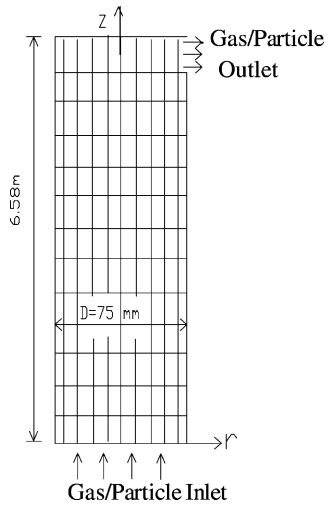

Fig. 1. Computational domain in the simulations.

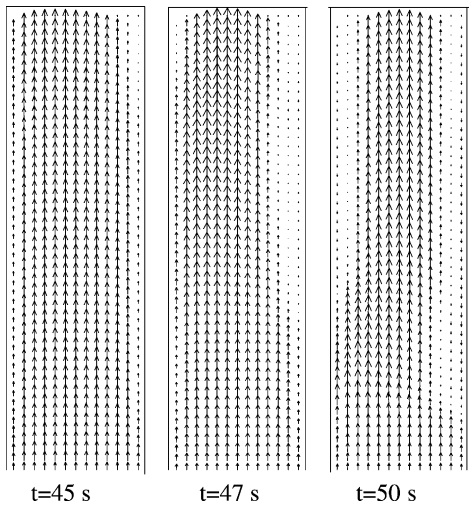

Fig. 2. Particle velocity fields in the simulations.

rapid parametric sensitivity analysis, while final quantitative validation should eventually be done in three dimensions (3D). In this simulation, a constant time step of 1.0×10^{-5} was used. Time-averaged distributions of flow variables are computed covering a period of 95 s corresponding to 1–2 weeks of computational time on a PC (20GB hard disk, 128 Mb RAM and of 600 MHz CPU). Hence, 3D computations, though more comprehensive and bringing more insight, are prohibitively time consuming. For this reason, only 2D computations are made here to evaluate parametric model sensitivity and associated trends.

3. Two-dimensional simulation results of gas–solids flow

3.1. Results and discussions

Several simulations have been performed in order to investigate the effect of different operating conditions, model assumptions, and to get an adequate description of the observed two-phase flow patterns in the riser of the CFB. Fig. 2 shows the particle velocity field at the three different times of 45, 47, and 50 s from the beginning of the simulation at gas velocity and solids mass flux of 2.61 m/s and 20.4 kg/(m^2 s), respectively. Strong flow heterogeneities as well as complex transitory velocity fields are evident from the computations (i.e. the velocity variation with diameter and height of riser, see Figs. 7 and 8). A characteristic feature of the flow is the oscillating motion of particles. Certain portions of the bed undergoes vigorous up and down motions, thus favoring a strong particle recirculation all over the riser. Fig. 3 shows the computed instantaneous local solids concentration as a function of time. At the begin of the simulations, the riser is considered as empty. Computations show that the riser will take about 25–30 s to fill up and come to a stable operating condition, thereafter.

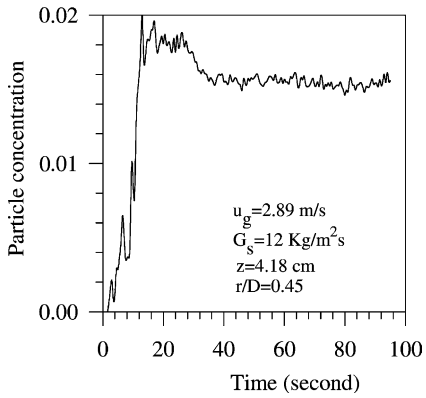

Fig. 3. Computed local instantaneous particle concentrations.

In order to compare simulation results with Miller and Gidaspow [8] data, time-averaged distributions of flow variables have been computed. Three riser sections, at 1.86, 4.18, and 5.52 m above the flow distributor, have been investigated. Fig. 4 shows the radial distribution of time-averaged

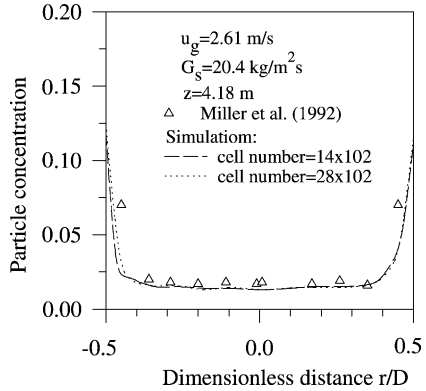

Fig. 4. Distribution of computed time–average particle concentration.

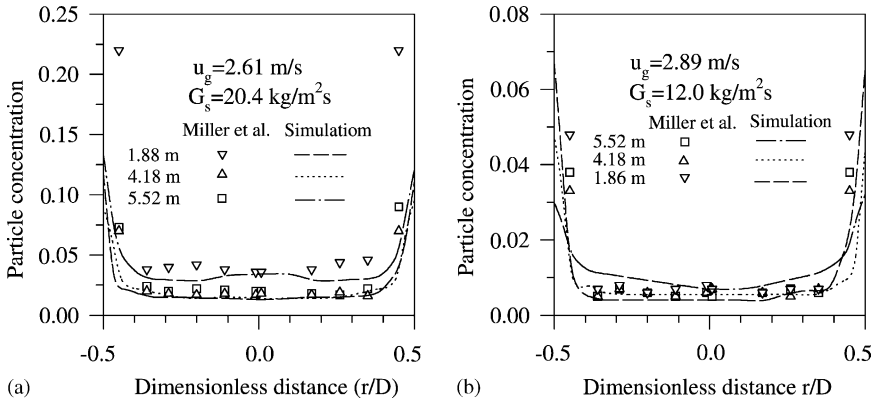

Fig. 5. Radial profiles of experimental and simulated particle concentrations.

particle concentrations for two difference cell numbers of 14×121 and 28×121. It can be seen that the computed results of coarse- and fine-cell are very similar and compare well with experimental data. Fig. 5a and b show comparisons between experimental and predicted solids concentrations across three sections over the time period 35–95 s. It can be seen that the particle concentrations are low in the center and high near the walls. The two simulations clearly illustrate the inherent core-annular pattern of the solids flow. The solids mainly accumulate and move downwards at the walls, whereas a dilute gas–particle stream flows upwards in the core of the riser. Fig. 6 shows the distributions of the cross-sectional averaged solid concentrations in the region of 0.0–2.0 m from the inlet of riser. The lower region of the riser is denser than the upper-dilute region even though the solids mainly accumulate at the walls in both the regions. As we can see from these diagrams, the model is able to describe quantitatively the accumulation of solid at the wall. Solid concentrations appear flat in the core and increase near the wall. Fig. 7 shows the simulated instantaneous axial velocity of particles as a function of time at the superficial gas velocity and mass flux of 2.61 m/s and 20.4 kg/(m^2 s), respectively. The positive values of axial particle velocities mean that the particles flow up in the center of riser, while the negative axial velocities of particles indicate that the particles flow down near the walls. Fig. 8a and b show comparisons between experimental and predicted particle velocities across three sections over the time period of 35–95 s. Regarding the axial solids velocity cross-section profiles, the comparison is less satisfactory overall, though well within an order of magnitude agreement. The core upward solids velocity acceleration is underestimated, whereas the solids down-flow velocity is predicted with a good approximation. In other words, the solids acceleration zone between 1.86 and 4.8 m is not well rendered by the computations. In contrast, the downward solids velocity does not seem to depend on the vertical region considered.

Tsuji et al. reported the measurements of gas and particle phases flow properties in a fully developed air–particle turbulent flow in a 30.5 mm vertical pipe by means of a laser–Doppler velocimeter (LDV) [27]. The polystyrene spheres with a density of 1020 kg/m^3 and averaged diameters of 0.2 and 0.5 mm were used in their experiments. A restitution coefficient of $e = 0.92$ for particle–particle collisions, and $e_w = 0.74$ for particle–wall collisions are used in the present study. These values are consistent with the

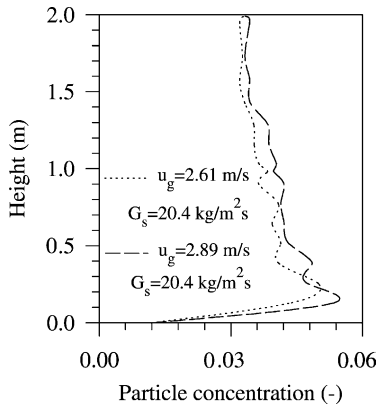

Fig. 6. Axial variations of radial averaged particle concentrations.

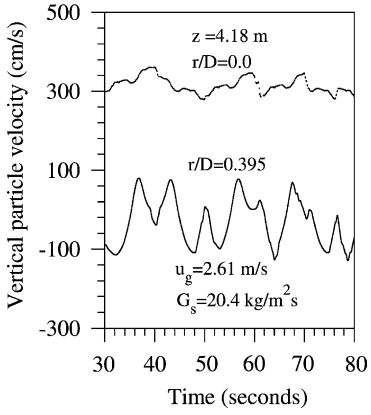

Fig. 7. Variations of instantaneous vertical particle velocity.

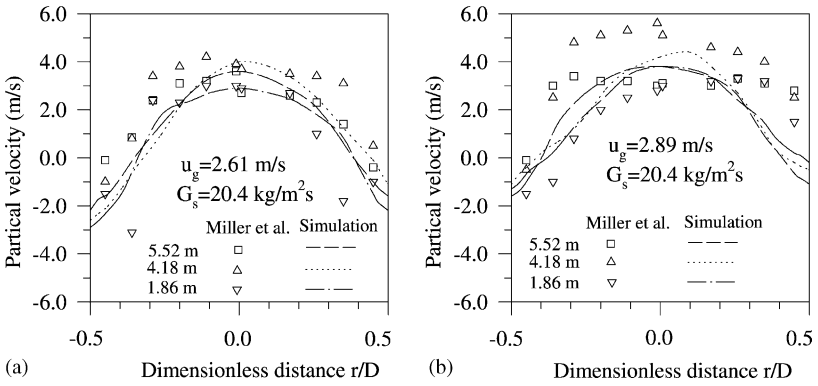

Fig. 8. Radial profiles of computed and experimental particle velocities.

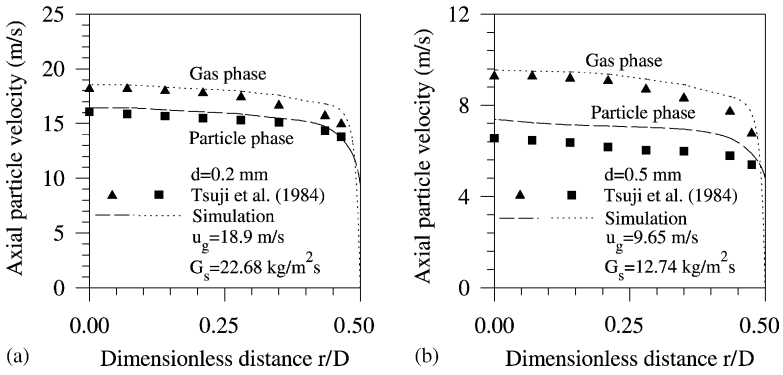

Fig. 9. Simulated and experimental axial particle velocities profiles.

observation of Govan et al. [28], who studied the trajectories of glass spheres transported in a small pipe under conditions similar to those of Tsuji et al. [27]. In the computations, the pressure gradient in the gas phase is input and is adjusted until the gas velocity at the centerline is within 1% of the experimentally measured values. The uniform distributions of inlet gas and particle velocities are assumed. The inlet particle concentration is calculated from measured mass loading of particles. Fig. 9a presents the model predictions for the flow conditions of air and 0.2 mm polystyrene sphere mixtures. Here, the mass loading ratio and the centerline gas velocity are 1.0 and 18.9 m/s, respectively. The computed gas velocity profile has a sharp gradient near the wall. The computed time-averaged axial particle velocity profile is quite flat across the pipe, with a significant relative velocity at the wall. This is because the air flow is subject to the no-slip condition at the wall, while the particle phase slips. It can be seen that the simulated gas and particle velocities are in agreement with the experimental data. Fig. 9b compares the predicted time-averaged axial particle and gas velocities for an air–polystyrene (0.5 mm) particle mixture with the experimental data of Tsuji et al. [27]. In this case, the mass loading ratio and air velocity are 1.1 and 9.65 m/s, respectively. It is observed that the predicted particle velocity is higher than the experimental results. The predictions of gas velocity are in agreement with the experimental data.

Figs. 10 and 11 show the time-averaged radial profiles of the granular temperature θ and solids pressure as computed by the kinetic theory model presented earlier, across the three sections described earlier. As we can see from the simulated results, the core region appears characterized by a granular temperature greater than in the denser annular regions. A reasonable agreement between predicted values and experimental data can be observed for granular temperature since experimental granular temperature values ranging between 0.5 and 2.0 (m/s)^2 have been measured at about 10 mm from the riser wall of this CFB for dense and dilute regimes

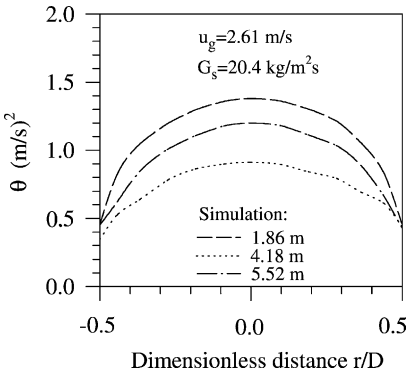

Fig. 10. Radial profiles of computed granular temperature.

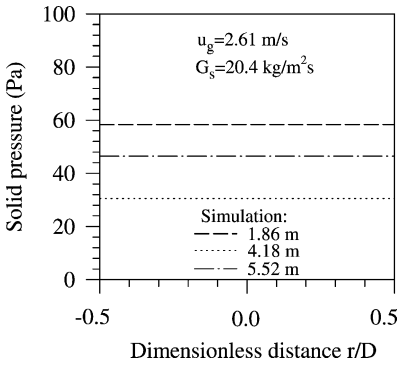

Fig. 11. Radial profile of computed solid pressure.

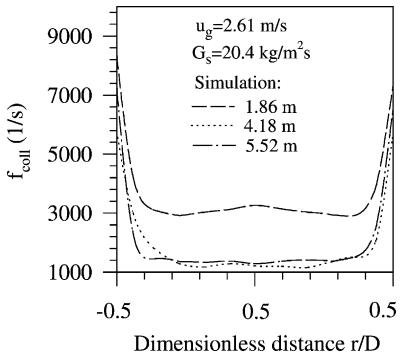

Fig. 12. Profile of computed collisional fequency of particles.

at similar operating conditions [29]. Regarding the particle pressure, we observe an almost uniform radial distribution of particle pressure across the riser with predicted values of about 30–60 Pa which are consistent with experimental values of about 50–100 Pa. obtained by Gidaspow and Huilin [26]. From the computed granular temperature and particle concentration, the collisional frequency of particles can be calculated based on the kinetic theory of granular flow [13]:

$$f_{\text{coll}} = 6.77\left(\frac{\varepsilon_s}{d}\right) g_o \sqrt{\theta} \tag{20}$$

Fig. 12 shows the distribution of the computed collisional frequency of particles at the gas velocity and solid mass flux of 2.61 m/s and 20.4 kg/(m^2 s), respectively. It can be seen that the collisional frequencies are higher near the wall than that in the center of riser. Although the granular temperature is low at the wall, the collisional frequency becomes high due to the high particle concentration. Although the granular temperatures are high in the center, the collisional frequencies are low because of low particle concentrations.

Fig. 13 shows the power spectrum density at different frequencies of oscillations in the riser. The Fourier transform method has been used to calculate the power spectrum of the particle concentration time series with a sampling time of 0.1 s. It can be seen that the main frequency of the particle concentrations lie within 0.07–0.2 Hz which corresponds to 10–15 s time period. A similar frequency has been reported by Neri and Gidaspow [20] using the kinetic theory approach for particulate phase. The main reason for calculating the frequency of oscillations of gas–solids flow was to know the minimum time required to conduct proper time averaging, in order to evaluate particle velocity standard deviations discussed below which enter in the definition of the total granular temperature.

The Eulerian gas–solids flow model is based on the kinetic theory for granular flow. In the derivation of this kinetic theory and its granular temperature definition, an isotropic behavior of the particle fluctuations is assumed. The governing equations come from interaction of the fluctuating and mean motion of the particles. The fluctuating velocity of particles obtained from the granular temperature is considered as the small-scale solids turbulence. Time-averaged experimental measurements always include small- and large-scale oscillations of particles. Therefore, a comparison between the computation and experimental data is possible only if the large-scale oscillations of particles are included. The large-scale oscillations of particles are essentially due to solids concentration fluctuations that are represented in Figs. 3 and 13. These fluctuations give rise to large-scale solids velocity oscillations which are to be

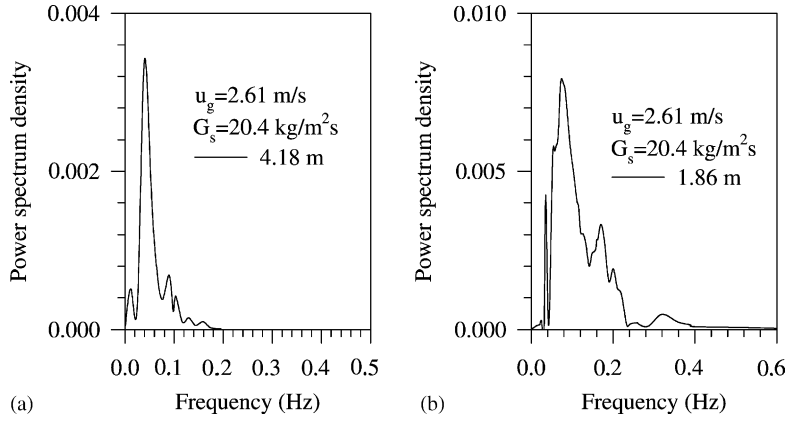

Fig. 13. Profiles of power spectrum density of predicted solids concentration using FFT method.

distinguished from the velocity fluctuations emanating from the kinetic theory. In our computations, both small-scale oscillations (represented by the granular temperature) and the large-scale oscillations (transient values of the solids velocity) are accounted for. If we hypothesize that the small- and large-scale fluctuations of particles are statistically independent (note that the large-scale oscillations have a frequency of about 0.1 Hz (see Fig. 13), whereas the small-scale frequency is of the order of 10–20 kHz [29]), a total granular temperature of particles, ϑ, can be defined assuming the angular and the radial velocity fluctuations to be equal in the 2D simulations [29] as:

$$\vartheta = \theta + (\tfrac{1}{3}\sigma_z^2 + \tfrac{2}{3}\sigma_x^2) \quad (21)$$

where the standard deviation σ of particle velocities is given by:

$$\sigma = \sqrt{\frac{1}{(N-1)}\sum_{i=1}^{N}(v_i - v_m)^2} \quad (22)$$

where v_i and v_m are the computed instantaneous particle velocity and mean particle velocity, respectively.

Fig. 14 shows the profile of the computed total granular temperature from small- and large-scale fluctuations of particles in any cell of the riser as a function of solids concentrations. The instantaneous particle velocity taken from the computed time series with a sampling time of 0.1 s after 35 s of run time to 80 s. The diagram shows that a simple relation between total granular temperature and solids concentration is not univocal. It is interesting to observe the variations of computed total granular temperature in the riser. A reasonable trend is shown between the predicted total granular temperature and the experimental data obtained by Gidaspow and Huilin [26]. First, a predicted maximum for a solids concentration of about 0.05–0.1 appears to be in agreement with that experimentally measured of about 0.03–0.08 by Gidaspow and Huilin [26]. The total granular temperature tends to increase with increasing solids concentrations in the

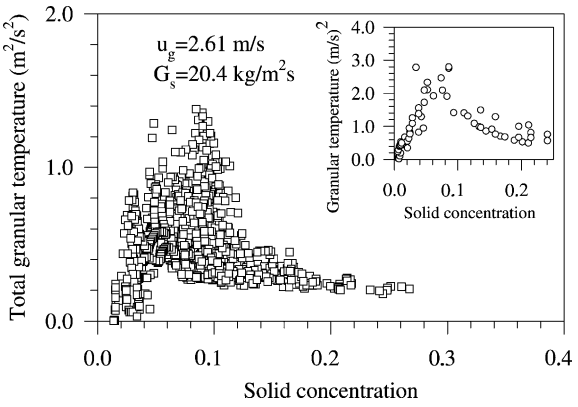

Fig. 14. Total computed granular temperature as a function of solid concentration in any cell of the computational domain. (The box shows the experimental granular temperature values from Gidaspow and Huilin (1998) [26]).

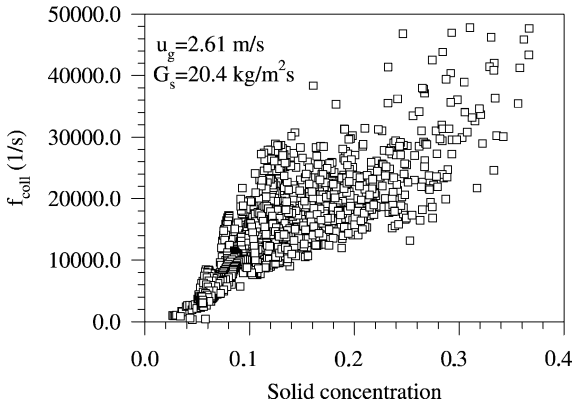

Fig. 15. Profile of collisional frequency as a function of solid concentration.

dilute region ($\varepsilon_s < 0.1$) and to decrease with an increase of solids concentration in the dense region ($\varepsilon_s > 0.1$). This behavior in the dilute regime was recently proved by Gidaspow and Huilin [26]. In fact, for a dilute gas–solids regime, the granular temperature is proportional to the solids concentration raised to the power of 2/3 [13]. In the dense regime, the decrease in the granular temperature is essentially due to the decrease of the mean free path of the particles. As the regime becomes that of the packed bed (high solids concentration), the granular temperature becomes vanishingly small. Our computed trends and magnitude of the total granular temperature agree with experimental data, though being overall somewhat smaller than experimental data.

Fig. 15 shows the profile of collisional frequency of particles as a function of particle concentration at the gas velocity and solid mass flux of 2.61 m/s and 20.4 kg/(m^2 s), respectively. The collisional frequency of particles increases with increasing solid concentration. The collisional frequency is higher at the high solid concentration than that at the low values of particle concentrations. As the solid concentration approaches to zero, the particle collisions became very low. This means the effect of particle interactions on the behavior of gas–solid flow can be neglected.

Fig. 16 shows the computed solids viscosity as a function of solids concentration in any cell of computational domain based on the calculated total granular temperature. The figure also shows the experimental granular viscosity measured by Gidaspow and Huilin [29]. Both empirical data and simulations exhibit the same trend as a function of solids concentration, with the computed solids viscosity being somewhat smaller than the experimental results. This is mainly due to the under-prediction of the total granular temperature in the simulations, as mentioned previously (see Fig. 14). In fact, the prediction of a more accurate granular temperature would lead to a more realistic prediction of solids viscosity and flow pattern of gas–solids flow in the riser. This granular temperature under-prediction may possibly be linked to the formulation of the solids velocity and granular temperature boundary conditions described by

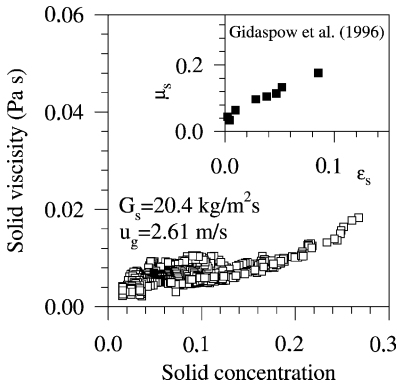

Fig. 16. Solids viscosity as a function of solid concentration in any cell of the computational domain.

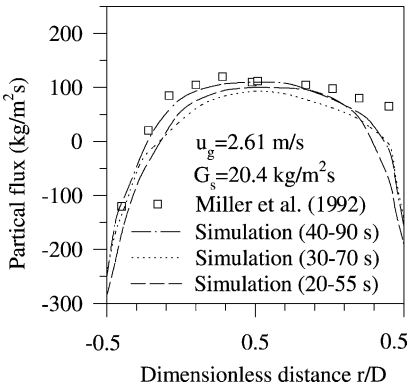

Fig. 18. Effect of initial conditions on the solid flux in the riser at the 4.18 m height.

Eqs. (19) and (20), as well as the 2D restrictions imposed in these simulations.

On the macroscopic scale of the particles, Hunt [30] proposed a correlation for the thermal conductivity as a function of the granular temperature:

$$K_s = \frac{\rho_s c_{p,s} d \pi^{3/2} \varepsilon_s \sqrt{\theta}}{32 g_o} \quad (23)$$

where $c_{p,s}$ is specific heat of particles. Fig. 17 shows the result of the effective solid phase thermal conductivity as a function of the solid concentration. It is obvious that the thermal conductivity of the solid phase increases for an increasing particle concentrations, since the number of particle contacts increases. Gidaspow and Syamlal [31] proposed a formulation of effective thermal conductivity of the solids phase and predicted heat transfer coefficients in the bubbling fluidized beds. From Fig. 17, it can be seen that the trends of the calculated effective thermal conductivity of the solids phase, with respect to solids concentrations, are similar, although those predicted in this work display higher values. To obtain an order-of-magnitude estimate for the solids heat transfer conductivity of this powder in the riser, one can evaluate from this figure a solids thermal conductivity of about 1.6 W/(m °C) for an average granular temperature

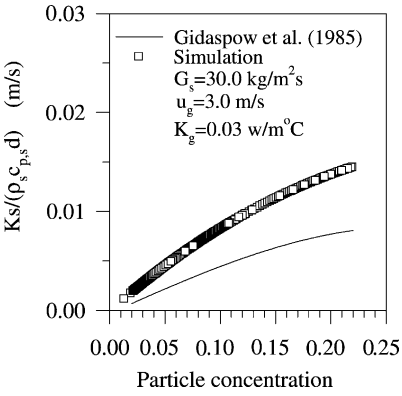

Fig. 17. Effective solid phase thermal conductivity as a function of the solid concentration in the riser.

of about 1.0 (m/s)^2 (see Fig. 10). This solids conductivity is about 50 times greater than that of the gas (0.03 W/(m °C)). Such high values may explain why CFB have excellent heat transfer characteristics. This model can readily provide the granular thermal conductivity of suspended powders which can be used to predict heat transfer phenomena in fluidized beds.

3.2. Effect of initial conditions

A case, where the particles initially fill the bottom of the riser to a height of 1.0 m at minimum fluidization conditions ($\varepsilon_{s,mf} = 0.4$), was considered. All the other initial and boundary conditions are the same as the previous case study. Fig. 18 shows the effect of initial conditions on the solids mass flux distribution in the riser at 4.18 m high compared with experimental data taken at the same height. At the beginning of the simulation, the solids initially present in the riser moved toward the wall region. This enhanced the particle flux at the walls in the beginning of the simulation. After a longer time, the newer particles fed through the riser bottom mix with the particles that were initially in the riser. There are no significant differences between this simulation and the previous one starting with an empty riser. Hence, the effect of the initial condition used in this simulation tends to disappear after several seconds of simulations. A quasi permanent regime is then reached.

3.3. Effect of inlet design

To investigate the effects of inlet design, an asymmetric solids inlet is considered, whereby solids particles are fed from one side-port of the riser, as it would be from a return leg. Fig. 19 shows the time-averaged solids flux at 4.18 m height in the riser compared to the experimental data at the same height. At this height of the riser, the solids flux was radially unsymmetric. A core-annular flow regime is still predicted with a much lower solids flux on one side of the riser. In such conditions, a detailed 3D simulation

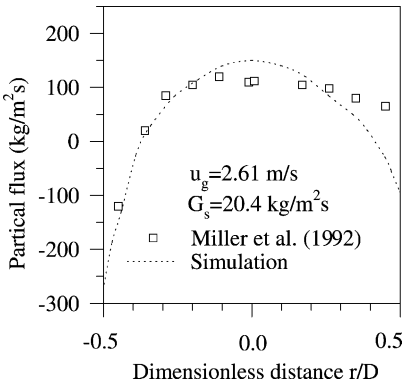

Fig. 19. Solid flux distribution at 4.18 m height in the riser with a solids side-port condition.

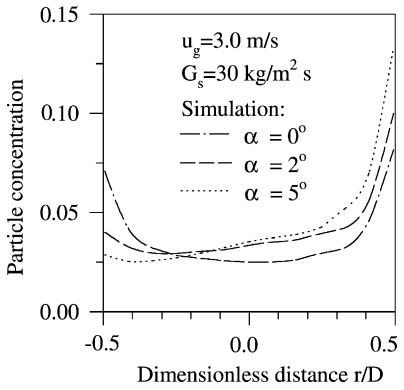

Fig. 21. Effect of inclined angles on solids concentrations in the riser at the 4.18 m height.

should be conducted to handle such complex geometries. This requires, on the other hand, very long computational times with today's computer capabilities, which remains the limiting factor for such computations.

3.4. Effects of riser diameter

To investigate the effect of larger riser diameters on the flow profile in the riser, a twice as large as 150 mm riser was considered. All other initial, inlet, and outlet conditions are the same as previously described in Fig. 1 and in Section 2.5. Fig. 20 shows a comparison of the particle concentration distributions in a 75 and 150 mm riser after 35 s of real time. The core-annular flow regime can be seen clearly in the figure since the core of both riser is more dilute than the near wall regions. The particle concentration remains high at the riser walls, and low in its center. An increase of riser diameter leads to an increase of particle concentrations at the riser walls and a particle concentration decrease in the center of riser. Hence, a change in the diameter of riser has incidence upon flow patterns of the riser and it, therefore, understood that the solids concentrations profiles obtained from a given geometry is generally not transferable to another.

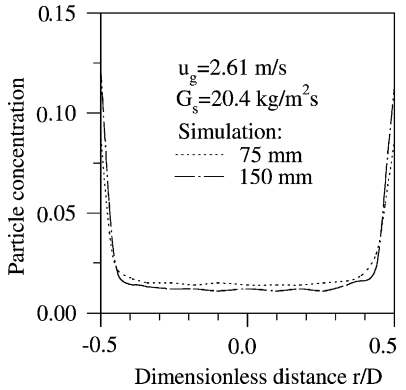

Fig. 20. Particle concentration distribution at 4.18 m height in a 75 and 150 mm riser.

3.5. Effects of riser inclination angles

With increased riser heights, it is often difficult to maintain risers in a vertical position. To investigate the effect of inclined angles on the flow profile in the riser, two cases of different inclined angles of 2 and 5° with vertical direction of riser were considered. Fig. 21 shows a comparison of the particle concentration distributions in the inclined angle of 0.0, 2.0 and 5.0° of riser at the superficial gas velocity and solid mass flux of 3.0 m/s and 30.0 kg/(m^2 s), respectively. For vertical risers (i.e. inclined angle of 0.0°), the solids concentration remains high at the riser walls and low in its center, displaying a core-annular flow regime. As the inclination angle increases, a substantial increase of particle concentrations at the lower side wall is displayed while particle concentration decreases in the upper side wall. Fig. 22 shows the solid flux distributions at inclined angle of 0.0, 2.0 and 5.0° for a superficial gas velocity and solid flux of 3.0 m/s and 30.0 kg/(m^2 s), respectively. This figure shows a strong influence of the inclination angle on the solids concentration and vertical mass fluxes between 0 and 2° while its influence being milder between 2 and 5°. The maximum solids flux is no longer at the center of the pipe but in the first quarter of the pipe diameter. Predicted negative solids

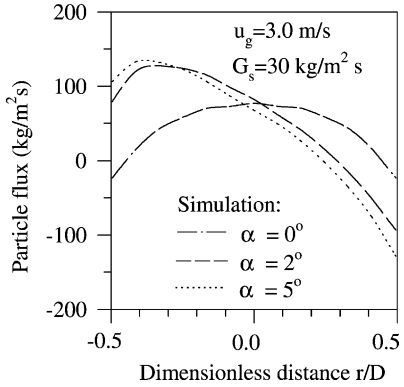

Fig. 22. Particle flux distribution in the riser at the 4.18 m height.

fluxes at the walls are no longer negative as in the case of strictly vertical pipes but become significantly positive on one side of the pipe and strongly negative on the other side by a factor of almost four-folds. This behavior is reminiscent of that found in Miller and Gidaspow [8] in their Fig. 16. Hence, a small change in the inclined angle of riser ($<2^\circ$) has a strong incidence upon the flow patterns of the riser. It is suspected that these effects become more pronounced as the riser height increases.

4. Conclusions

A 2D transient model incorporating the kinetic theory for the particulate phase was capable of predicting reasonably well the main features of the complex gas–solids flow behavior in the riser. The time-averaged core-annular flow, experimentally observed in the dense riser flows, was successfully predicted by this model. It is understood, however, that this vision is only valid on a time averaged basis, because in reality there is a continuous up- and down-flow motions occurring at frequency of about 10 Hz thereby yielding large vortices. Such frequencies were predicted with the proposed model and were experimentally validated. Unexpected strong flow distortions due to a few degrees riser inclination were shown to lead to a shift of the maximum solids mass flux from the center of the pipe to the first quarter of the pipe and to the change of mass flux direction (negative to positive) on one side of the pipe as well as a four-folds increase in the negative solids mass flux on the other side.

Note that low order discrepancies still persisting may be due in part to the effects of electrostatic effects, particle cohesiveness, and multi-size particle distribution. To treat such details, the kinetic theory presented here should be extended for multi-size particles and investigated using 3D simulations. As such, detailed 3D inlet and exit design effects should be considered. Computer capacity still remains, however, the major limiting factor to simulate gas–solids flow for such complex geometries.

Considering the imperfections of the present kinetic theory model, predicted trends are, however, considered to be reasonably good with respect to available experimental measurements. Small-scale hydrodynamics features such as local granular pressures and temperatures, yielding high solids thermal conductivity, are readily predictable from the theory and could be used to investigate heat transfer phenomena in CFBs.

Acknowledgements

This work was partially supported by the National Science Foundation in China through Grant no. 10072019 and USA National Science Foundation through Grant no. CTS-0086250.

References

[1] J.F. Davidson, Symposium on fluidization: discussion, Trans. Inst. Chem. Eng. 39 (1961) 230.
[2] H. Arastoopour, D. Gidaspow, Vertical pneumatic conveying using four hydrodynamic model, Ind. Eng. Chem. Fundam. 18 (1979) 123–133.
[3] Y.P. Tsuo, D. Gidaspow, Computation of flow patterns in circulating fluidized beds, AIChE J. 36 (1990) 885–893.
[4] R.W. Lyczkowsky, I.K. Gamwo, F. Dobran, H. Ali, B.T. Chao, M. Chao, M. Chen, D. Gidaspow, Validation of computed solids hydrodynamics and pressure oscillation in bubbling atmospheric fluidized bed, Powder Technol. 76 (1993) 65–76.
[5] K.S. Anderson, S. Sundaresan, R. Jackson, Instabilities and the formation of bubbles in fluidized beds, J. Fluid Mech. 303 (1995) 327–344.
[6] S. Benyahia, H. Arastoopour, T.M. Knowlton, H. Maddah, Simulation of particles and gas flow behavior in the riser section of a circulating fluidized bed using the kinetic theory approach for the particulate phase, in: Proceedings of the Advanced Technology for Particle Processing, AIChE, New York, 1998, pp. 477–484.
[7] B. Sun, D. Gidaspow, Computation of circulating fluidized bed riser flow for the fluidization. Part VIII: Benchmark test, Ind. Eng. Chem. Res. 38 (1999) 787–792.
[8] A. Miller, D. Gidaspow, Dense, vertical gas–solids flow in a pipe, AIChE J. 38 (1992) 1801–1813.
[9] S. Champan, T.J. Cowling, The Mathematical Theory of Non-Uniform Gases, Cambridge University Press, London, 1961.
[10] C.K.K. Lun, S.B. Savage, D.J. Jeffrey, N. Chepurnity, Kinetic theory for granular flow: inelastic particles in Couette flow and slightly inelastic particles in a general flow field, J. Fluid Mech. 140 (1984) 223–235.
[11] J.L. Sinclair, R. Jackson, Gas–particle flow in a vertical pipe with particle–particle interactions, AIChE J. 35 (1989) 1473–1486.
[12] J. Ding, D. Gidaspow, A bubbling fluidization model using kinetic theory of granular flow, AIChE J. 36 (1990) 523–538.
[13] D. Gidaspow, Multiphase Flow and Fluidization: Continuum and Kinetic Theory Descriptions, Academic Press, New York, 1994.
[14] M.Y. Louge, E. Mastorakos, J.T. Jenkins, The role of particle collisions in pneumatic transport, J. Fluid Mech. 231 (1991) 345–359.
[15] J.A. Pita, S. Sundareasan, Gas–solids flow in vertical tubes, AIChE J. 37 (1992) 1009–1018.
[16] C.M. Hrenya, J.L. Sinclair, Effects of particle–particle turbulence in gas–solids flows, AIChE J. 43 (1997) 853–871.
[17] A. Samuelsberg, B.J.H. Hjertager, Computational modeling of gas–particle flow in a riser, AIChE J. 42 (1996) 1536–1547.
[18] J.J. Nieuwland, M. Van Sint Annaland, A.M. Kuipers, P.M. Van Swaaij, Hydrodynamic modeling of gas–particle flows in riser reactors, AIChE J. 42 (1996) 1569–1582.
[19] G. Balzer, O. Simonin, A. Boelle, J. Lavieville, A unifying modeling approach for the numerical prediction of dilute and dense gas–solid flow, in: Proceedings of the Circulating Fluidized Bed V, 1996, Beijing, China, MSD6 (preprint).
[20] A. Neri, D. Gidaspow, Riser hydrodynamics: simulation using kinetic theory, AIChE J. 46 (2000) 52–67.
[21] J. Cao, G. Ahmadi, Gas–particle two-phase turbulent flow in a vertical duct, Int. J. Multiphase Flow 21 (1995) 1203–1228.
[22] J.W. Deardorff, On the magnitude of the sub-grid scale Eddy coefficient, J. Comput. Phys. 7 (1971) 120–127.
[23] R.A. Bagnold, Experiments on a gravity-free dispersion of large solids spheres in a Newtonian fluid under shear, Proc. Roy. Soc. A225 (1954) 49–63.
[24] D.L. Koch, Kinetic theory for a mono-disperse gas–solids suspension, Phys. Fluids A 2 (1990) 1711–1723.
[25] S.V. Patankar, Numerical heat transfer and fluid flow, Hemisphere, New York, 1980.

[26] D. Gidaspow, L. Huilin, Equation of state and radial distribution function of FCC particles in a CFB, AIChE J. 44 (1998) 279–293.
[27] Y. Tsuji, Y. Morikawa, H. Shiomi, LDV measurements of an air–solid two-phase flow in a vertical pipe, J. Fluid Mech. 139 (1984) 417–437.
[28] A.H. Govan, G.F. Hewitt, C.F. Ngan, Particle motion in the turbulent pipe flow, Int. J. Multiphase Flow 15 (1989) 471–481.
[29] D. Gidaspow, L. Huilin, Collisional viscosity of FCC particles in a CFB, AIChE J. 42 (1996) 2503–2510.
[30] M.L. Hunt, Discrete element simulations for granular material flows: effective thermal conductivity and self-diffusivity, Int. J. Heat Mass Trans. 40 (1997) 3059–3068.
[31] D. Gidaspow, M. Syamlal, Hydrodynamics of fluidization prediction of wall to heat transfer coefficients, AIChE J. 31 (1985) 127–135.